Modeling Competitive Interactions in Proteins: Vibrational Spectroscopy of M^+(*n*-methylacetamide)$_1(H_2O)_{n=0-3}$, M = Na and K, in the 3 μm Region†

Dorothy J. Miller and James M. Lisy*

University of Illinois at Urbana-Champaign, Urbana, Illinois 61801

Received: May 8, 2007; In Final Form: June 28, 2007

To properly understand the preferred structures and biological properties of proteins, it is important to understand how they are influenced by their immediate environment. Competitive intrapeptide, peptide···water, ion···water, and ion···peptide interactions, such as hydrogen bonding, play a key role in determining the structures, properties, and functionality of proteins. The primary types of hydrogen bonding involving proteins are intramolecular amide···amide (N−H···O═C) and intermolecular amide···water (O−H···O═C and H−O···H−N). *n*-Methylacetamide (NMA) is a convenient model for investigating these competitive interactions. An analysis of the IR photodissociation (IRPD) spectra of M^+(*n*-methylacetamide)$_1(H_2O)_{n=0-3}$ (M = Na and K) in the O−H and N−H spectral regions is presented. Ab initio calculations (MP2/cc-pVDZ) are used as a guide in identifying both the type and location of hydrogen bonds present. In larger clusters, where several structural isomers may be present in the molecular beam, ab initio calculations are also used to suggest assignments for the observed spectral features. The results presented offer insight to the nature of ion···NMA interactions in an aqueous environment and reveal how different ion···ligand pairwise interactions direct the extent of water···water and water···NMA hydrogen bonding observed.

1. Introduction

The hydration of amide functional groups is of fundamental interest due to their prevalence in biological macromolecules. To properly characterize the preferred structures and biological properties of proteins and peptides, it is important to understand the noncovalent interactions between the amide functional group and its immediate environment. The primary hydrogen-bonding interactions involving peptides are intramolecular amide···amide (N−H···O═C) and intermolecular amide···water (O−H···O═C and H−N···O−H). *n*-Methylacetamide (NMA), which contains an amide group, is a tractable model for investigating competitive interactions involving the peptide backbone. As such, it has been and continues to be an opportune system for both experimental[1−12] and theoretical[13−24] study.

It has recently been shown that strong water···solute hydrogen bonds significantly influence the shape and solute charge distribution of biologically important species and, since shape and biological activity of biomolecules are intimately related, solvating waters are an integral part of functional biological systems.[25−32] These distributions are also influenced by charged species in close proximity.[33−39] Sodium and potassium cations are among the most abundant metal ions found in biological systems, with concentrations on the order of ∼100 mM.[40] As such, these cations are involved in a variety of processes: osmotic balance, the stabilization of biomolecular conformations, and transfer via ion pumps and ion channels. It has recently been shown in this lab and others that strong, electrostatic ion···ligand interactions perturb the hydrogen-bonding motif and structures of neutral hydrated biomodels.[41−45] In indole, the aromatic chromophore of tryptophan, the proximity of a potassium cation shifted the primary hydrogen-bonding site from the indole N−H group to the π-cloud of the pyrrole ring of indole.[44] A recent study by the groups of Williams and Rizzo[41] demonstrated the effect of a lithium cation on the hydration and structure of the amino acid valine.

Gas-phase IR vibrational spectroscopy is a powerful tool for systematically probing the onset of hydrogen bonding. The N−H stretching vibration of NMA and the O−H stretching vibrations of water are particularly sensitive to their local environment and, as such, these modes are useful probes of specific cation···water···NMA interactions. An experimental and theoretical study by our group demonstrated that the O−H stretching modes of the gas-phase water monomer shift to lower frequency in binary $M^+(H_2O)_1$ complexes and that the magnitude of this shift was proportional to the strength of the ion···water interaction.[46] Water O−H stretching modes are further shifted upon hydrogen-bond formation, with the magnitude of this shift relative to the strength of the hydrogen bond formed.[47−50] Recently, Köddermann and Ludwig, using FTIR spectroscopy,[6] Zhang et al., using IR spectroscopy,[12] and Czarnecki and Haufa, using generalized two-dimensional FT-NIR,[2] have shown that the different NMA···water hydrogen-binding motifs, C═O···H−O vs N−H···O−H, are identifiable through shifts in the X−H stretching vibrations. In the present work, we investigate the effect of a strong electrostatic interaction on NMA···water hydrogen bonding.

2. Technical Details

2.1. Experimental Method. Our experimental apparatus, described elsewhere,[51−53] consists of a source chamber, where cluster ions are generated, and a detection chamber, where the ions are mass-selected, fragmented, and then mass-analyzed. Briefly, neutral clusters are generated in a supersonic expansion of an argon carrier gas seeded with NMA and water through a 180 μm, 45° conical nozzle. Water vapor is picked up by the

† Part of the "Giacinto Scoles Festschrift".

* To whom correspondence should be addressed. E-mail: j-lisy@uiuc.edu.

10.1021/jp073521i CCC: $37.00
Published on Web 08/16/2007

TABLE 1: Experimental and Theoretical (MP2/LANL2DZ for Na and K/cc-pVDZ for N, C, O, and H) Binding Energies in kcal/mol for the $M^+(NMA)_1(H_2O)_{n=0-1}$, M = K and Na, and NMA(H_2O) Cluster Constituents

	theoretical[a]					
	ΔE_E	ΔE_0	$\Delta H_{298.15}$	$T\Delta S_{298.15}$	$\Delta G_{298.15}$	experimental[b]
NMA···H_2O (C═O···H−O) trans to C−N bond	−10.3	−7.8	−8.4	−9.3	1.0	
NMA···H_2O (C═O···H−O) C−N bond eclipsed	−10.2	−7.7	−8.2	−9.2	0.9	
NMA···H_2O (N−H···O−H)	−8.7	−6.8	−7.0	−8.7	1.7	
K^+···NMA	−27.2	−26.3	−25.1	4.0	−29.1	*−28.3*/**−30.4**
K^+(NMA)···H_2O	−17.5	−16.2	−16.0	−5.4	−10.6	
Na^+···NMA	−39.9	−38.7	−37.6	3.0	−40.6	*−33.7*/**−35.7**
$Na^+(NMA)_1$···H_2O	−25.9	−24.4	−24.4	−6.2	−18.1	

[a] This work. *trans*-NMA was used in each binding energy calculation. [b] Reference 5, experimental threshold CID ΔH_{298} values indicated by *italic*/**bold** fonts. Values in italics were obtained with kinetic shift corrections carried out with the two lowest frequencies arbitrarily set at 30 cm^{-1}. Bolded values were obtained with the two lowest frequencies set at 10 cm^{-1} for Na^+ and 5 cm^{-1} for K^+ (experimental uncertainty was ± 3 kcal/mol).The latter values were considered the better ones.

carrier gas when argon is passed through a bubbler containing deionized water. Gaseous NMA is introduced inside the experimental apparatus prior to the supersonic expansion by passing the H_2O/Ar mixture through a heated (∼40 °C) sample holder containing NMA.

Approximately 150 nozzle diameters downstream from the nozzle, an ion beam (either Na^+ or K^+ produced via thermionic emission from a homemade ion gun) perpendicularly intersects the fully expanded molecular beam. This collision, along with subsequent ion solvation, forms an ensemble of unstable cluster ions with high internal energies. Through rearrangement and progressive loss of solvating molecules, as described by the evaporative ensemble,[54−56] the nascent cluster ions lose both mass and internal energy until they are quasi-stable and the cluster lifetime is long compared with the time required to completely traverse the detection chamber.

After cluster formation, an octapole ion guide or a set of electrostatic lenses guide the ion clusters to the first of three quadrupoles, where the cluster ions of interest are mass-selected. The mass-selected species then enter the second r.f.-only quadrupole where, if a photon from one of our tunable IR lasers ($LiNbO_3$ optical parametric oscillator pumped by a 20 Hz Nd:YAG or LaserVision OPO/OPA pumped by a 10 Hz Surelite II, both systems have ∼2 cm^{-1} resolution) is absorbed, the cluster ions fragment. The remaining parent ions and resulting fragment ions are mass analyzed in the third quadrapole. The photoacoustic spectrum of ambient water vapor is simultaneously recorded for absolute frequency calibration. Reported IR photodissociation (IRPD) spectra have been smoothed with a three-point averaging algorithm.

2.2. Computational Method. Where needed, ab initio geometries and harmonic vibrational frequencies and thermodynamic analyses of changes in free energy as a function of temperature were used in interpreting the experimental spectra and identifying the types of noncovalent interactions present. Preliminary structures were generated with Spartan 02[57] using a molecular mechanics geometry optimization with the Merck Molecular Force Field. These were then refined with GAUSSIAN 03[58] and the B3LYP/6-31+G* basis and theory. Low-lying isomers (isomers within 3 kcal/mol of the global minimum) were further optimized at the second-order Møller−Plesset (MP2) level of theory with the cc-pVDZ basis set. LANL2DZ effective core potentials were used for potassium, as the cc-pVDZ basis set is not available, and sodium, for consistency.

Binary binding energies, reported in Table 1, and harmonic vibrational frequencies were calculated at the MP2/cc-PVDZ theory and basis, as dispersive interactions, and zero-point vibrational energies (ZPEs) are expected to be important when evaluating binary interactions in ionic clusters. Theoretical spectra were generated using the SWizard plotting program[59] with an applied average Gaussian peak width and of 15 cm^{-1} for N−H modes and 20 cm^{-1} for O−H modes. A linear scaling factor of 0.9543 was applied to facilitate comparison between the experimental and theoretical spectra.[60]

Nascent cluster ions produced in our experiments have a significant amount of internal energy due to the formation process—the collision between an ion and a preformed neutral cluster. These cluster ions cool through progressive evaporative loss of solvent molecules until they reach a quasi-stable state, allowing for an estimate of the internal energy to be calculated. Theoretical binding energies, experimental cluster ion flight times, and unimolecular dissociation rates (calculated using RRK and RRKM methods) were used to estimate effective cluster ion temperatures. For both $Na^+(H_2O)$Ar and $K^+(H_2O)$Ar cluster ions,[46] the estimated and experimental temperatures were in good agreement, supporting this method of characterizing cluster ion internal energies. The effective temperature of $Na^+(CH_3OH)_{3-8}$ cluster ions has been estimated to be on the order of 250−300 K.[54] $M^+(NMA)_1(H_2O)_{1-4}$ clusters are expected to cool primarily through the evaporative loss of water molecules. Because the K^+(NMA)···H_2O (16.2 kcal/mol, Table 1) and Na^+(NMA)···H_2O (24.4 kcal/mol, Table 1) interactions are of similar magnitude as the Na^+···CH_3OH interaction (26.4 kcal/mol),[54] the effective temperature of $M^+(NMA)_1(H_2O)_n$ cluster ions should also be in the 250−300 K range. In this temperature range, entropic effects can have a significant impact on the energetic ordering of low-lying cluster isomers. Entropic and enthalpic effects were evaluated using the thermo.pl[61] PERL script and taken into consideration when evaluating the energetic ordering of low-lying isomers at experimental temperatures.

3. Results and Discussion

3.1. $M^+(NMA)_1$Ar. Before we can investigate hydration in our NMA model system, we must first understand the electrostatic interaction between NMA and the sodium or potassium cation. A strong M^+···NMA binding energy (26.3 kcal/mol for K^+ and 38.7 kcal/mol for Na^+)[5,11] prevents direct IRPD measurements. Instead, the argon-messenger technique, wherein an argon atom is weakly bound to the ion cluster, was used.[62−64] Previous experiments using this tagging technique showed that incorporation of argon into the ion cluster does not perturb X−H stretching modes.[46]

The IRPD spectra of $K^+(NMA)_1$Ar and $Na^+(NMA)_1$Ar are shown in Figures 1 and 2, respectively. These spectra are qualitatively identical: a single feature near 3485 cm^{-1}. In neutral NMA studies, features in this spectral region have been identi-

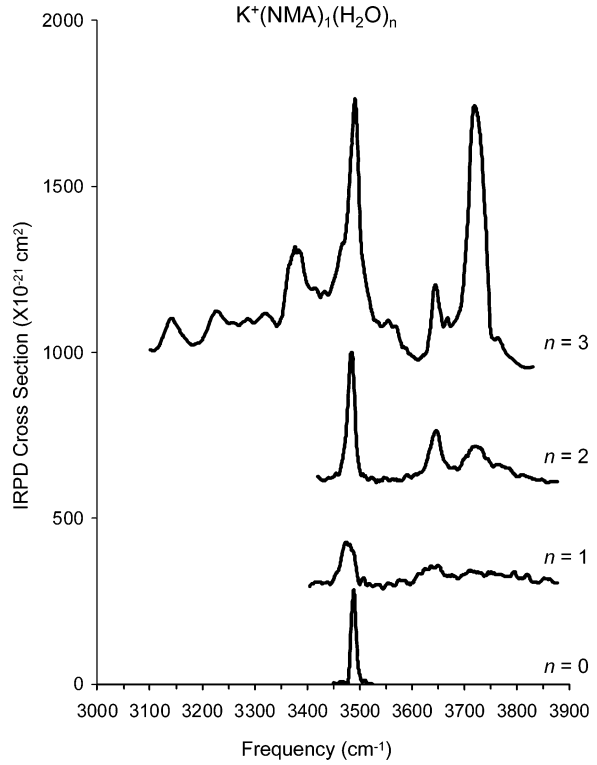

Figure 1. IRPD of $K^+(NMA)_1(H_2O)_n$, $n = 0-3$.

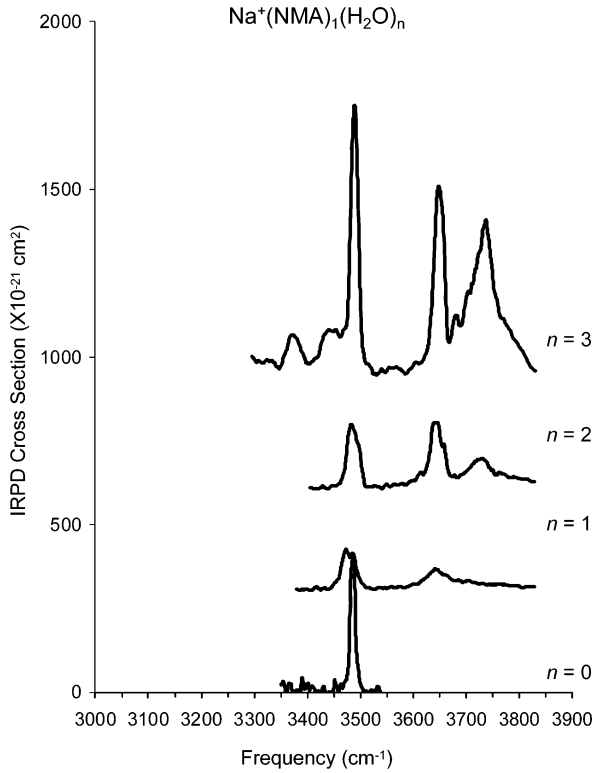

Figure 2. IRPD of $Na^+(NMA)_1(H_2O)_n$, $n = 0-3$.

fied as the free N−H stretching vibration of either *trans*-NMA (∼3470 cm^{-1}) or *cis*-NMA (∼3435 cm^{-1}).[1,4,6,10] The *trans*-NMA isomer is predicted to be more stable (∼2.4 kcal/mol)[3,8,19] than the *cis*-NMA, as reflected by the low (∼1−3%)[1,4,6,10] abundance of *cis*-NMA observed. The free N−H vibrations of the two isomers are split by approximately 38 cm^{-1},[1,4,6,10] well within the resolution limit of our experimental apparatus. Therefore, because only one N−H stretch is observed in the $M^+(NMA)_1Ar$ spectra, only the *trans*-NMA isomer is present in the $M^+(NMA)_1Ar$ ion clusters. Ab initio geometry calculations of the $M^+(NMA)_1$ cluster indicate that both the sodium and potassium cation interact with NMA via the carbonyl group; minimum energy structures are shown in Figure 3.

Complexation with a cation shifts the position of the neutral *trans*-NMA free N−H vibration roughly 14 cm^{-1} higher in frequency. This shift is due to a perturbation of the N−H stretch by the electrostatic interaction with the cation. There is a 5 cm^{-1} difference in the frequency of the N−H stretch in $K^+(NMA)_1$-Ar (3488 cm^{-1}) and in $Na^+(NMA)_1Ar$ (3483 cm^{-1}). This difference is again reflective of frequency perturbation due to the proximity of a cation.

3.2. $M^+(NMA)_1(H_2O)_{1,2}$. When neutral NMA is hydrated, two types of NMA···H_2O hydrogen-bonding interactions may occur, an N−H···O−H hydrogen bond and/or a C═O···H−O hydrogen bond. The different hydrogen-bonding motifs, C═O···H−O vs N−H···O−H, are identifiable by the separate spectral shifts they incite.[2,6,12] When the N−H group is involved in a NMA···H_2O hydrogen bond, the N−H stretch is shifted ∼25 cm^{-1} lower in frequency with little perturbation to the O−H oscillators.[6] When a C═O···H−O hydrogen bond is formed, a free O−H feature near 3686 cm^{-1} and a hydrogen-bonded O−H feature at 3470 cm^{-1} are observed.[6] The interaction between the C═O group and water is stronger than the interaction between the N−H group and water and, therefore, C═O···H−O hydrogen-bond formation is favored over N−H···O−H hydrogen-bond formation. Even in water-rich environments, a free N−H oscillator is favored over a N−H···O−H hydrogen bond.[2,6,12] When the $M^+(NMA)_1$ cluster ion is initially hydrated, strong ion···dipole interactions are expected to dominate over the above-mentioned NMA···H_2O hydrogen-bonded interactions. Hydrogen bonds are expected in the $M^+(NMA)_1(H_2O)_n$ clusters only when the electrostatic interaction is comparable in strength with the hydrogen bond.

The $K^+(NMA)(H_2O)_{1-2}$ and $Na^+(NMA)(H_2O)_{1-2}$ spectra, shown in Figures 1 and 2, respectively, are, again, qualitatively identical. In each spectrum, three features are observed. The feature near 3480 cm^{-1} is assigned, as before, to the *trans*-NMA free N−H stretch. The two features to higher frequency are assigned to the asymmetric (∼3720 cm^{-1}) and the symmetric (∼3640 cm^{-1}) O−H stretches of the hydrating water(s). These features are moderately shifted (∼36 cm^{-1} and ∼17 cm^{-1}, respectively) from the water monomer transitions at 3756 cm^{-1} (asymmetric O−H) and 3657 cm^{-1} (symmetric O−H).[65] This O−H shift is, again, indicative of the ion perturbation. None of the observed features have the characteristic shifts indicating hydrogen-bond formation, suggesting that, in these small hydrated cluster ions, the strong ion···H_2O electrostatic interaction precludes NMA···H_2O hydrogen-bond formation. This assessment is supported by the calculated minimum energy structures, see Figure 3, which show the water molecule(s) and the NMA individually interacting with the ion without NMA···water or, in the case of $M^+(NMA)_1(H_2O)_2$, water··· water interactions.

3.3. $M^+(NMA)_1(H_2O)_3$. Differences are observed between the $K^+(NMA)_1(H_2O)_3$ and the $Na^+(NMA)_1(H_2O)_3$ spectra, specifically below 3600 cm^{-1} in the hydrogen-bonding region. At this larger cluster size, NMA···H_2O and H_2O···H_2O hydrogen-bonding interactions are competitive with ion···NMA and ion···H_2O electrostatic interactions. In many cases, the hydrogen-bonded features, either O−H or N−H, are in close spectral

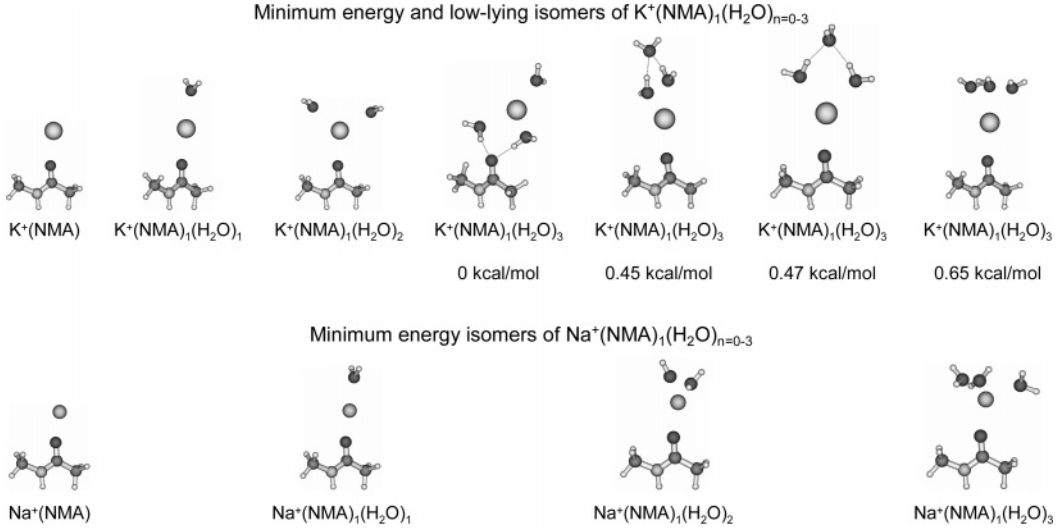

Figure 3. Minimum energy isomers of $M^+(NMA)_1(H_2O)_n$, $n = 0-3$, and additional low-lying isomers of $K^+(NMA)_1(H_2O)_3$.

proximity and, with an estimated cluster temperature near 300 K, these hydrogen-bonded features may be spectrally overlapped.

To better resolve the features in the hydrogen-bonding region, we employed a cooling technique wherein neutral $(NMA)_m$-$(H_2O)_n$ clusters are generated using a very lean water concentration and high argon backing pressure. As mentioned earlier, NMA is incorporated into the neutral cluster via a pick-up technique just prior to supersonic expansion. Therefore, the water-to-argon ratio does not affect the concentration of gaseous NMA. The combination of low water vapor to high argon gas in the supersonic expansion is expected to produce clusters that cool primarily through evaporation of argon (although loss of water and/or NMA may also occur), thereby, generating cooler clusters with lower internal energy than those formed primarily through evaporation of water molecules. The density of argon-tagged $M^+(NMA)_1(H_2O)_{3,4}$ cluster ions, though present in the mass spectrum, was insufficient for using the argon-messenger technique.

3.3.1. $K^+(NMA)_1(H_2O)_3$. Through comparison with the smaller $K^+(NMA)_1(H_2O)_{0-2}$ clusters, the *trans*-NMA N−H feature (∼3488 cm^{-1}) and the non-hydrogen-bonded symmetric O−H feature (∼3644 cm^{-1}) are again identified. However, the other non-hydrogen-bonded O−H feature (∼3716 cm^{-1}) is slightly shifted to lower frequency, is narrower, and has greater IR intensity relative to the symmetric O−H feature. These changes suggest that the feature near 3716 cm^{-1} is comprised of two components, the asymmetric O−H stretch and a free O−H stretch.[66] Free O−H stretching features appear when one of the two O−H oscillators in water acts as a proton donor in a hydrogen bond while the other O−H oscillator remains free (not involved in hydrogen bonding). Thus, the presence of a free O−H feature is an additional indicator of hydrogen bonding. Because the symmetric O−H feature is still present, not all of the water molecules are involved in O−H hydrogen bonding. Conversely, because the free O−H feature is present, O−H hydrogen-bonding exists in the $K^+(NMA)_1(H_2O)_3$ clusters. With three water molecules present in the cluster ion, both water···water and NMA···water O−H hydrogen bonding may occur.

To identify the type of O−H hydrogen bonding present, we looked at the five new features in the hydrogen-bonding region, starting with the two features observed near 3137 and 3227 cm^{-1}. These features are lower in frequency than where

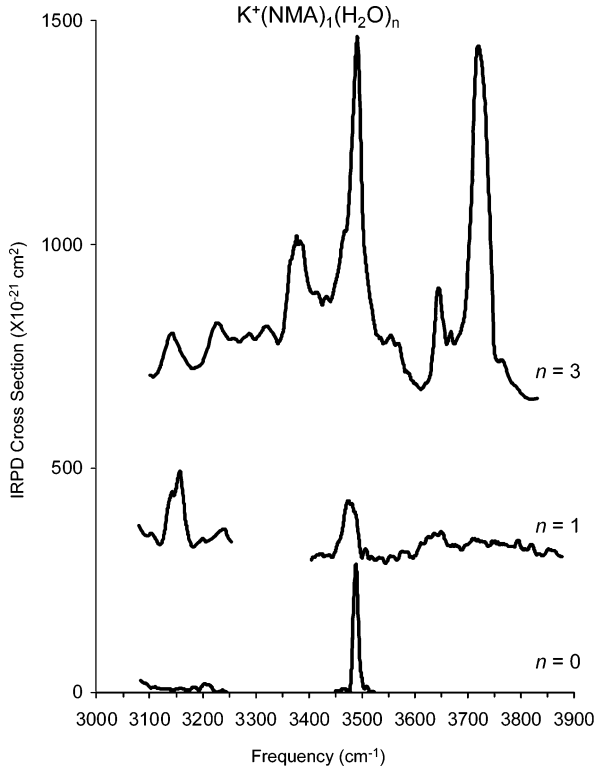

Figure 4. IRPD spectrum of $K^+(NMA)_1(NMA)_3$ compared with the $K^+(NMA)_1Ar$ and $K^+(NMA)_1(H_2O)_1Ar$ spectra in the 3300−3000 cm^{-1} region.

either water···water or NMA···H_2O O−H hydrogen-bonded stretching features are expected. In fact, these features do not correspond with the fundamental stretching frequency of any $K^+(NMA)_1(H_2O)_3$ cluster constituent. However, the vibrational overtone of the C═O stretch (fundamental near 1710 cm^{-1})[1,4,7] and/or the vibrational overtone of the H−O−H bend (fundamental near 1658 cm^{-1})[47,50,67] are expected in this region. To identify which vibrational overtone gives rise to the features observed, the relevant spectral region of the $K^+(NMA)_1Ar$ and the $K^+(NMA)_1(H_2O)_1Ar$ spectra need to be compared with the $K^+(NMA)_1(H_2O)_3$ spectrum as is shown in Figure 4. Clearly, there are no features present in the $K^+(NMA)_1Ar$ spectrum, indicating that the features observed in the $K^+(NMA)_1(H_2O)_3$

spectrum are not associated with the C═O stretching overtone. The prominent feature observed near 3143 cm^{-1} in the $K^+(NMA)_1(H_2O)_1Ar$ spectrum corresponds to the lower frequency feature in the $K^+(NMA)_1(H_2O)_3$ spectrum, identifying it as the non-hydrogen-bonded H−O−H bend overtone. The second feature, observed near 3226 cm^{-1} in the $K^+(NMA)_1(H_2O)_3$ spectrum, is assigned to the hydrogen-bonded H−O−H bend overtone. This hydrogen-bonded feature is shifted to higher frequency due to the stiffening of the bending vibration when an O−H hydrogen bond is formed.[47]

Three more O−H hydrogen-bonded assignments remain. A weak feature near 3560 cm^{-1} is observed near where water···water bent hydrogen bonding was observed in hydrated $K^+(H_2O)_n$ clusters.[68] While suggestive, this comparison does not unambiguously identify the feature near 3560 cm^{-1} as a bent water···water hydrogen-bond feature. A theoretical analysis of possible low-lying isomers is needed to pose a positive assignment for this feature. The shoulder (near 3464 cm^{-1}) on the low-frequency side of the N−H stretching vibration and the feature near 3377 cm^{-1} do not correspond with previously observed water···water hydrogen-bonding vibrations. However, they are located below 3600 cm^{-1}, in the O−H hydrogen-bonded spectral region, and are therefore indicative of O−H hydrogen bonding. The only other type of O−H proton-donating hydrogen bond that may form in $K^+(NMA)_1(H_2O)_3$ clusters is an O−H···O═C hydrogen bond. For this type of hydrogen bond to be observed, an isomer with a second shell NMA secured via C═O···H−O hydrogen bond(s) must be present in the ionic beam. An analysis of the low-lying isomers is again needed to identify which structures are energetically favorable under our experimental conditions.

To help assign the features observed near 3560, 3464, and 3377 cm^{-1}, the low-lying isomers for $K^+(NMA)_1(H_2O)_3$ were located and their geometries and vibrational frequencies calculated (MP2/cc-pVDZ). Only isomers within 1 kcal/mol ZPE corrected energy of the minimum energy isomer are discussed. Theoretical geometries and spectra of the low-lying $K^+(NMA)_1(H_2O)_3$ isomers are shown in Figures 3 and 5A, respectively. With and without ZPE correction, the predicted minimum energy isomer shows the three water molecules occupying the first solvent shell and NMA occupying the second solvent shell, secured with two C═O···H−O hydrogen bonds to two first shell water molecules. The harmonic vibrational frequencies associated with the two C═O···H−O hydrogen bonds, after scaling, are in good agreement with the observed features in the $K^+(NMA)_1(H_2O)_3$ spectrum. The splitting between the C═O···H−O hydrogen-bonded features observed, both experimentally (∼87 cm^{-1}) and theoretically (∼48 cm^{-1}), is attributed to differing water···NMA interactions. The higher frequency feature (∼3464 cm^{-1}) comes from the C═O···H−O hydrogen bond eclipsing the NMA C−N bond while the lower frequency feature (∼3377 cm^{-1}) comes from the water molecule trans to the NMA C−N bond. From this, the two O−H hydrogen-bonded features (3464 and 3377 cm^{-1}) observed in the $K^+(NMA)_1(H_2O)_3$ spectrum are assigned to C═O···H−O hydrogen bonding.

Two isomers, differing only in the orientation of the bent water···water hydrogen bond relative to the NMA, lie slightly higher in energy (∼0.45 and ∼0.47 kcal/mol). Both of these closely related isomers contain water···water bent hydrogen bonds that give rise to an O−H hydrogen-bonded feature near 3593 cm^{-1}. Approximately 0.65 kcal/mol higher in energy than the minimum energy isomer lies an isomer with all four ligands in the first solvent shell. In this isomer, each of the water

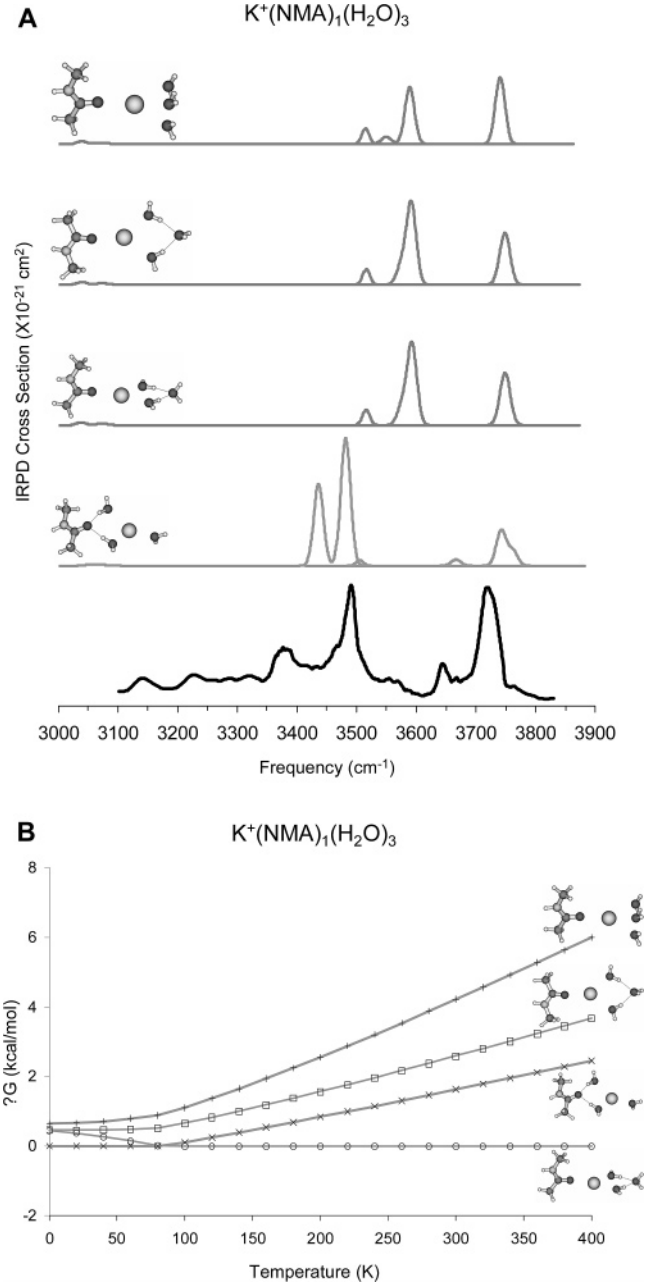

Figure 5. (A) Experimental and theoretical spectra with structures of the four low-lying $K^+(NMA)_1(H_2O)_3$ isomers. (B) Change in free energy (kcal/mol) as a function of temperature (K) for the four low-lying isomers of $K^+(NMA)_1(H_2O)_3$: C═O···H−O hydrogen-bonded isomer ×, perpendicular water···water bent hydrogen-bonded isomer ○, parallel water···water bent hydrogen-bonded isomer □, and cyclic water trimer hydrogen-bonded isomer +.

molecules is involved in a hydrogen bond with an adjacent water molecule forming a cyclic water trimer. Such a hydrogen-bonded network also gives rise to an O−H hydrogen-bonded feature near 3590 cm^{-1}.

The experimental $K^+(NMA)_1(H_2O)_3$ cluster ion is considerably warmer than 0 K and, while the theoretical analysis thus far has yielded isomers in agreement with the experimental spectrum, entropic contributions need to be accounted for to make a more definite assignment of the feature observed near 3560 cm^{-1}. The change in free energy with respect to temperature for the four low-lying isomers is plotted in Figure 5B. At low temperatures, the isomers are energetically ordered as in the discussion above. As the temperature increases, however, a

reordering occurs. Near 80 K, the C═O···H−O hydrogen-bonded isomer and the isomer with the bent water···water hydrogen bond perpendicular to NMA switch places: there are no other re-orderings at the temperatures evaluated. Near room temperature, the isomer containing the cyclic water trimer hydrogen-bonded network has become increasingly less stable and is now ∼4 kcal/mol higher in energy than the minimum energy bent water···water hydrogen-bonded isomer. Therefore, the feature near 3560 cm^{-1} is assigned primarily to the bent water···water hydrogen-bonded vibration.

3.3.2. $Na^+(NMA)_1(H_2O)_3$. The most obvious difference between the $Na^+(NMA)_1(H_2O)_3$ spectrum and the $K^+(NMA)_1(H_2O)_3$ spectrum is that the $Na^+(NMA)_1(H_2O)_3$ spectrum lacks a water···water bent hydrogen-bonded feature near 3560 cm^{-1}. The lack of O−H hydrogen bonding is also reflected in the symmetric (3647 cm^{-1}) and asymmetric (3737 cm^{-1}) O−H features where the two features have approximately the same IR intensity and are very similar to the symmetric and asymmetric O−H features observed in the $Na^+(NMA)_1(H_2O)_2$ spectrum. The similarity of IR intensity between the two features indicates that the majority of O−H oscillators in the $Na^+(NMA)_1(H_2O)_3$ cluster ions are not involved in hydrogen bonding. However, some O−H hydrogen bonding does occur as the two C═O···H−O hydrogen-bonded features are again observed near 3443 and 3368 cm^{-1}. These features are slightly lower in frequency relative to those observed in the $K^+(NMA)_1(H_2O)_3$ spectrum and the splitting between the features is reduced (∼75 cm^{-1}). As in other instances where shifts in IR frequency are observed between potassium and sodium containing cluster ions, this frequency shift and difference in C═O···H−O splitting is an artifact of the Na^+···ligand interaction.

The theoretical structure and spectrum of the low-lying $Na^+(NMA)_1(H_2O)_3$ isomer are shown in Figures 3 and 6A, respectively. In calculations (MP2/cc-pVDZ) of the $Na^+(NMA)_1(H_2O)_3$ cluster ion, there are no low-lying isomers within 1 kcal/mol ZPE corrected energy of the minimum energy isomer. The minimum energy isomer is a non-hydrogen-bonded isomer with all four ligands in the first solvent shell without water···water or NMA···water hydrogen-bonded interactions. Such a structure agrees with the experimental spectrum of $Na^+(NMA)_1(H_2O)_3$, which suggests that a large percentage of the water molecules are not involved in O−H hydrogen bonding. However, the experimental spectrum also indicates that C═O···H−O hydrogen-bonded isomers are present and that water···water hydrogen-bonded isomers are not present in the ionic beam.

Two higher energy, hydrogen-bonded isomers were located: a bent water···water hydrogen-bonded isomer (2.89 kcal/mol) and a C═O···H−O hydrogen-bonded isomer (3.03 kcal/mol), structures and spectra are shown in Figure 6A. An isomer, containing bent water···water hydrogen bonding—perpendicular to the NMA, an isomer with the bent water···water hydrogen bond parallel to the NMA was not located—and an isomer with C═O···H−O hydrogen bonding. An isomer with a cyclic hydrogen-bonded network, such as the one located in the $K^+(NMA)_1(H_2O)_3$ system, was not located for $Na^+(NMA)_1(H_2O)_3$. The difference between the observed and the calculated low-lying structures may be understood by accounting for entropic effects. Because there was insufficient intensity to use the argon-tagged $Na^+(NMA)_1(H_2O)_3Ar$ cluster ions for IRPD spectroscopy, we cannot guarantee that the cluster ions form solely via argon evaporation. However, due to the expansion conditions, the $Na^+(NMA)_1(H_2O)_3$ cluster ions are thought to form primarily through evaporative loss of argon with little, if any, water and/or NMA evaporations. Clusters formed solely by evaporation of argon have an estimated terminal temperature close to 50 K. Those formed solely by evaporation of water have an estimated terminal temperature near 300 K. Therefore, the experimental $Na^+(NMA)_1(H_2O)_3$ cluster ions should have a temperature between 50−300 K. The change in free energy as a function of temperature is plotted in Figure 6B. Near 100 K the two hydrogen-bonded isomers, water···water bent and C═O···H−O hydrogen-bonded, switch ordering, with the C═O···H−O hydrogen-bonded isomer becoming increasingly more stable than the bent water···water hydrogen-bonded isomer with increasing temperatue.

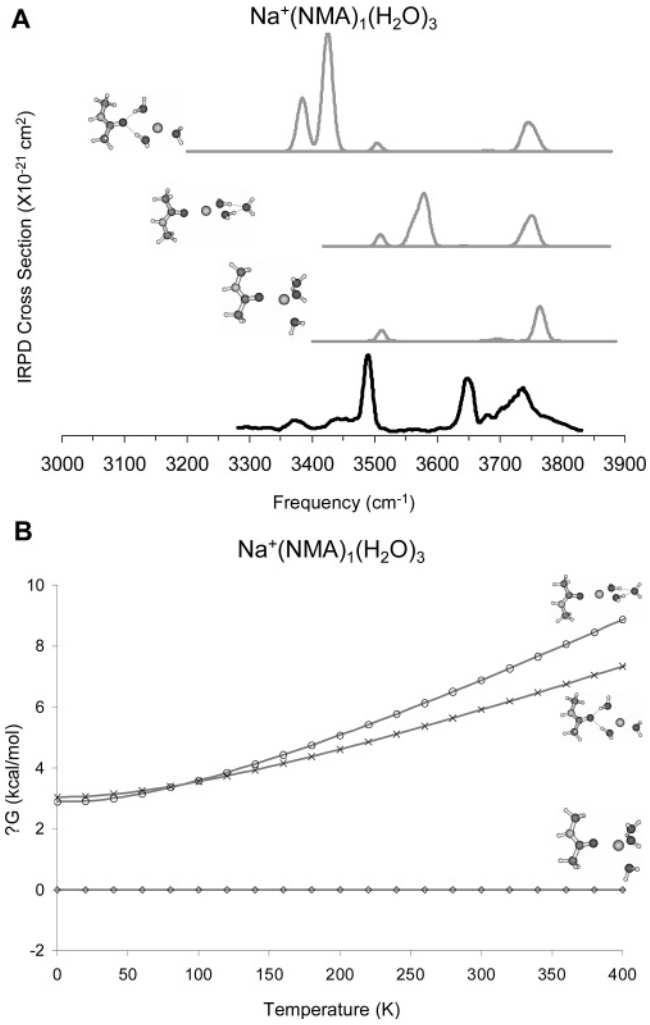

Figure 6. (A) Experimental and theoretical spectra with structures of three low-lying $Na^+(NMA)_1(H_2O)_3$, isomers. (B) Change in free energy (kcal/mol) as a function of temperature (K) for the three low-lying isomers of $Na^+(NMA)_1(H_2O)_3$: non-hydrogen-bonded isomer ◇, perpendicular water···water bent hydrogen-bonded isomer ○, and C═O···H−O hydrogen-bonded isomer ×.

Clearly, the non-hydrogen-bonded $Na^+(NMA)_1(H_2O)_3$ isomer is favored from both an enthalpic and entropic prospective. Evaluating the low-lying isomers with respect to the estimated cluster temperature and re-ordering the low-lying isomers to reflect that temperature bring the theoretic predictions and the experimental observations into better agreement: both non-hydrogen-bonded and C═O···H−O hydrogen-bonded isomers are present but hydrogen bonding is occurring only in a small percentage of the cluster ions sampled. If any water···water bent hydrogen-bonded isomers were formed, the low number of

contributing hydrogen-bonded O−H oscillators was insufficient to resolve this feature from the background noise.

4. Conclusions

For both the potassium and the sodium cation, the electrostatic cation···*n*-methylacetamide interaction was through the carbonyl group. With three or more water molecules present in the cluster, NMA was promoted to the ion's second coordination shell and secured with two O−H···O═C hydrogen bonds in a fraction of the ensemble. This is the only type of hydrogen bonding observed for sodium containing cluster ions, where stronger ion···ligand pairwise interactions are present. In the $K^+(NMA)_1(H_2O)_3$ clusters, where weaker ion···ligand pairwise interactions are present, both NMA···H_2O and water···water hydrogen-bonded signatures are observed. In the $K^+(NMA)_1(H_2O)_3$ clusters, theoretical analysis of this cluster showed that hydrogen bonding was present in each of the low-lying isomers. A low-lying isomer without either water···water or water···NMA hydrogen bonding was not located.

The experimental results for $M^+(NMA)_1(H_2O)_{n=0-3}$ agreed nicely with ab initio calculations for each cluster size. Neither water···water nor water···NMA hydrogen bonding were predicted nor observed for $M^+(NMA)_1(H_2O)_{n=0-2}$. Water···NMA hydrogen bonding was predicted and observed in the $M^+(NMA)_1(H_2O)_3$ cluster ions. The observance of C═O···H−O hydrogen-bonded features suggests that the preferred hydrogen-bonding topology of neutral $NMA(H_2O)_n$—where C═O···H−O hydrogen bonds are observed prior to N−H···H−O hydrogen bonds—was not affected by the electrostatic influence of either cation. N−H···O−H hydrogen bonding was not observed at the cluster sizes examined. This agrees with previous neutral experiments showing the N−H group non-hydrogen-bonded even in water-rich environments.[2,6,12]

Acknowledgment. This material is based on work supported by the National Science Foundation under Grant Nos. CHE-0415859 and CHE-0072178. We thank the donors to the Petroleum Research Fund of the American Chemical Society for financial support. Appreciation is also extended to Ms. Natalie Rebacz and Dr. Timothy Vaden for experimental and computational assistance.

References and Notes

(1) Ataka, S.; Takeuchi, H.; Tasumi, M. *J. Mol. Struct.* **1984**, *113*, 147.
(2) Czarnecki, M. A.; Haufa, K. Z. *J. Phys. Chem. A* **2005**, *109*, 1015.
(3) Herrebout, W. A.; Clou, K.; Desseyn, H. O. *J. Phys. Chem. A* **2001**, *105*, 4865.
(4) Jones, R. L. *J. Mol. Spectrosc.* **1963**, *11*, 411.
(5) Klassen, J. S.; Anderson, S. G.; Blades, A. T.; Kebarle, P. *J. Phys. Chem.* **1996**, *100*, 14218.
(6) Koddermann, T.; Ludwig, R. *Phys. Chem. Chem. Phys.* **2004**, *6*, 1867.
(7) Mayne, L.; Hudson, B. *J. Phys. Chem.* **1991**, *95*, 2962.
(8) Radzicka, A.; Pedersen, L.; Wolfenden, R. *Biochemistry* **1988**, *27*, 4538.
(9) Rubtsov, I. V.; Wang, J.; Hochstrasser, R. M. *J. Phys. Chem. A* **2003**, *107*, 3384.
(10) Russell, R. A.; Thompson, H. W. *Spectrochim. Acta* **1956**, *8*, 138.
(11) Tsang, Y.; Siu, F. M.; Ho, C. S.; Ma, N. L.; Tsang, C. W. *Rapid Commun. Mass Spectrom.* **2004**, *18*, 345.
(12) Zhang, R.; Li, H.; Lei, Y.; Han, S. *J. Mol. Struct.* **2004**, *693*, 17.
(13) Bour, P.; Keiderline, T. A. *J. Chem. Phys.* **2003**, *119*, 11253.
(14) Dannenberg, J. J. *J. Phys. Chem. A* **2006**, *110*, 5798.
(15) Dixon, D. A.; Dobbs, K. D.; Valentini, J. J. *J. Phys. Chem.* **1994**, *98*, 13435.
(16) Gregurick, S. K.; Chaban, G. M.; Gerber, R. B. *J. Phys. Chem. A* **2002**, *106*, 8696.
(17) Guo, H.; Karplus, M. *J. Phys. Chem.* **1992**, *96*, 7273.
(18) Han, W.-G.; Suhai, S. *J. Phys. Chem.* **1996**, *100*, 3942.
(19) Jorgensen, W. L.; Gao, J. *J. Am. Chem. Soc.* **1988**, *110*, 4212.
(20) Kubelka, J.; Keiderline, T. A. *J. Phys. Chem. A* **2001**, *105*, 10922.
(21) Langley, C. H.; Allinger, N. L. *J. Phys. Chem. A* **2003**, *107*, 5208.
(22) Schmidt, J. R.; Corcelli, S. A.; Skinner, J. L. *J. Chem. Phys.* **2004**, *121*, 8887.
(23) Torii, H. *J. Phys. Chem. A* **2004**, *108*, 7272.
(24) Yang, Z.-Z.; Qian, P. *J. Chem. Phys.* **2006**, *125*, 064311.
(25) Carney, J. R.; Dian, B. C.; Florio, G. M.; Zwier, T. S. *J. Am. Chem. Soc.* **2001**, *123*, 5596.
(26) Florio, G. M.; Zwier, T. S. *J. Phys. Chem. A* **2003**, *107*, 974.
(27) Guo, H.; Karplus, M. *J. Phys. Chem.* **1994**, *98*, 7104.
(28) Liu, D.; Wyttenbach, T.; Barran, P. E.; Bowers, M. T. *J. Am. Chem. Soc.* **2003**, *125*, 8458.
(29) Liu, D.; Wyttenbach, T.; Bowers, M. T. *Int. J. Mass Spectrom.* **2004**, *236*, 81.
(30) Robertson, E.; Simons, J. P. *Phys. Chem. Chem. Phys.* **2001**, *3*, 1.
(31) Snoek, L. C.; Kroemer, R. T.; Simons, J. P. *Phys. Chem. Chem. Phys.* **2002**, *4*, 2130.
(32) Zwier, T. S. *J. Phys. Chem. A* **2001**, *105*, 8827.
(33) Cerda, B. A.; Wesdemiotis, C. *Analyst* **2000**, *125*, 657.
(34) Dunbar, R. C. *J. Phys. Chem. A* **2000**, *104*, 8067.
(35) Feng, W. Y.; Gronert, S.; Lebrilla, C. *J. Phys. Chem. A* **2003**, *107*, 405.
(36) Jockush, R. A.; Lemoff, A. S.; Williams, E. R. *J. Am. Chem. Soc.* **2001**, *123*, 12255.
(37) Kish, M.; Ohanessian, G.; Wesdemiotis, C. *Int. J. Mass Spectrom.* **2003**, *227*, 509.
(38) Remko, M.; Rode, B. M. *J. Phys. Chem. A* **2006**, *110*, 1960.
(39) Wyttenbach, T.; Witt, M.; Bowers, M. T. *J. Am. Chem. Soc*. **2000**, *122*, 3458.
(40) Overman, R. R.; Davis, A. K. *J. Biol. Chem.* **1947**, *168*, 641.
(41) Kamariotis, A.; Boyarkin, O. V.; Mercier, S. R.; Beck, R. D.; Bush, M. F.; Williams, E. R.; Rizzo, T. R. *J. Am. Chem. Soc.* **2005**, *128*, 905.
(42) Lemoff, A. S.; Bush, M. F.; Williams, E. R. *J. Am. Chem. Soc*. **2003**, *125*, 13576.
(43) Lemoff, A. S.; Williams, E. R. *J. Am. Soc. Mass Spectrom.* **2004**, *15*, 1014.
(44) Miller, D. J.; Lisy, J. M. *J. Chem. Phys.* **2006**, *124*, 184301.
(45) Rogalewicz, F.; Hoppilliard, Y.; Ohanessian, G. *Int. J. Mass Spectrom.* **2003**, *227*, 439.
(46) Vaden, T. D.; Weinheimer, C. J.; Lisy, J. M. *J. Chem. Phys.* **2004**, *121*, 3102.
(47) Paul, J. B.; Provencal, R. A.; Chapo, C.; Roth, K.; Casaes, R.; Saykally, R. J. *J. Phys. Chem. A* **1999**, *103*, 2972.
(48) Huisken, F.; Kaloudis, M.; Kulcke, A. *J. Chem. Phys.* **1995**, *104*, 17.
(49) Jeffrey, G. A. *An Introduction to Hydrogen Bonding*; Oxford University Press: New York, 1997.
(50) Xantheas, S. S.; Dunning, T. H. *J. Chem. Phys.* **1993**, *99*, 8774.
(51) Draves, J. A.; Luthey-Schulten, Z.; Liu, W.-L.; Lisy, J. M. *J. Chem. Phys.* **1990**, *93*, 4589.
(52) Weinheimer, C. J.; Lisy, J. M. *J. Phys. Chem.* **1996**, *100*, 15305.
(53) Weinheimer, C. J.; Lisy, J. M. *Int. J. Mass Spectrom. Ion Process.* **1996**, *159*, 197.
(54) Cabarcos, O. M.; Weinheimer, C. J.; Lisy, J. M. *J. Phys. Chem. A* **1999**, *103*, 8777.
(55) Klots, C. E. *J. Chem. Phys.* **1985**, *83*, 5854.
(56) Klots, C. E. *Lett. Nat.* **1987**, *327*, 222.
(57) Kong, J.; White, C. A.; Krylov, A. I.; Sherrill, C. D.; Adamson, R. D.; Furlani, T. R.; Lee, M. S.; Lee, A. M.; Gwaltney, S. R.; Adams, T. R.; Ochsenfeld, C.; Maslen, A. T. B.; Dombroski, J. P.; Dashel, H.; Zhang, W.; Korambath, P. P.; Baker, J.; Byrd, E. F. C.; Voorhis, T. V.; Oumi, M.; Hirata, S.; Hsu, C.-P.; Ishikawa, N.; Florian, J.; Warshel, A.; Johnson, B. G.; Gill, P. M. W.; Head-Gordon, M.; Pople, J. A. *SPARTAN'02*; Wavefunction, Inc: Irvine, CA, 2002.
(58) Frisch, M. J.; Trucks, G. W.; Schlegel, H. B.; Scuseria, G. E.; Robb, M. A.; Cheeseman, J. R.; Montgomery, J. A., Jr.; Vreven, T.; Kudin, K. N.; Burant, J. C.; Millam, J. M.; Iyengar, S. S.; Tomasi, J.; Barone, V.; Mennucci, B.; Cossi, M.; Scalmani, G.; Rega, N.; Petersson, G. A.; Nakatsuji, H.; Hada, M.; Ehara, M.; Toyota, K.; Fukuda, R.; Hasegawa, J.; Ishida, M.; Nakajima, T.; Honda, Y.; Kitao, O.; Nakai, H.; Klene, M.; Li, X.; Knox, J. E.; Hratchian, H. P.; Cross, J. B.; Adamo, C.; Jaramillo, J.; Gomperts, R.; Stratmann, R. E.; Yazyev, O.; Austin, A. J.; Cammi, R.; Pomelli, C.; Ochterski, J. W.; Ayala, P. Y.; Morokuma, K.; Voth, G. A.; Salvador, P.; Dannenberg, J. J.; Zakrzewski, V. G.; Dapprich, S.; Daniels, A. D.; Strain, M. C.; Farkas, O.; Malick, D. K.; Rabuck, A. D.; Raghavachari, K.; Foresman, J. B.; Ortiz, J. V.; Cui, Q.; Baboul, A. G.; Clifford, S.; Cioslowski, J.; Stefanov, B. B.; Liu, G.; Liashenko, A.; Piskorz, P.; Komaromi, I.; Martin, R. L.; Fox, D. J.; Keith, T.; Al-Laham, M. A.; Peng, C. Y.; Nanayakkara, A.; Challacombe, M.; Gill, P. M. W.; Johnson, B.; Chen, W.; Wong, M. W.; Gonzalez, C.; Pople, J. A. *Gaussian 03*, B.04 ed.; Gaussian, Inc.: Pittsburg, PA, 2003.
(59) Gorelsky, S. I. *SWizard program*, 4.1 ed.; York University, Toronto, Canada, 2005; http://www.sg-chem.net/.

(60) Sinha, P.; Boesch, S. E.; Gu, C.; Wheeler, R. A.; Wilson, A. K. *J. Phys. Chem. A* **2004**, *108*, 9213.
(61) Irikura, K. K. *THERMO.PL*; National Institute of Standards and Technology, Gaithersburg, MD, 2002.
(62) Bieske, E. J.; Dopfer, O. *Chem. Rev.* **2000**, *100*, 3963.
(63) Duncan, M. A. *Int. Rev. Phys. Chem.* **2003**, *22*, 407.
(64) Robertson, W. H.; Johnson, M. A. *Annu. Rev. Phys. Chem.* **2003**, *54*, 173.
(65) Fraley, P. E.; Rao, K. N. *J. Mol. Spectrosc.* **1969**, *29*, 312.
(66) Weinheimer, C. J.; Lisy, J. M. *J. Chem. Phys.* **1996**, *105*, 2938.
(67) Verdes, D.; Linnartz, H. *Chem. Phys. Lett.* **2002**, *355*, 538.
(68) Miller, D. J.; Lisy, J. M. *J. Chem. Phys.* **2006**, *124*, 024319.